Axial force measurement of the bolt/nut assemblies based on the bending mode shape frequency of the protruding thread part using ultrasonic modal analysis

Measurement 162 (2020) 107914

Contents lists available at ScienceDirect

Measurement

journal homepage: www.elsevier.com/locate/measurement

Axial force measurement of the bolt/nut assemblies based on the bending mode shape frequency of the protruding thread part using ultrasonic modal analysis

Naoki Hosoya [a,*], Takanori Niikura [b], Shinji Hashimura [a], Itsuro Kajiwara [c], Francesco Giorgio-Serchi [d]

[a] Department of Engineering Science and Mechanics, Shibaura Institute of Technology, 3-7-5 Toyosu, Koto-ku, Tokyo 135-8548, Japan
[b] Division of Mechanical Engineering, Shibaura Institute of Technology, 3-7-5 Toyosu, Koto-ku, Tokyo 135-8548, Japan
[c] Division of Human Mechanical Systems and Design, Hokkaido University, N13, W8, Kita-ku, Sapporo 060-8628, Japan
[d] Scottish Microelectronics Centre, University of Edinburgh, Edinburgh EH9 3FF, United Kingdom

ARTICLE INFO

Article history:
Received 30 December 2019
Received in revised form 24 April 2020
Accepted 28 April 2020
Available online 11 May 2020

Keywords:
Axial force
Fastening force
Bolt/nut assembly
Protruding thread part
Vibration mode shape
Impact testing
Frequency response function
Modal analysis

ABSTRACT

Bolt/nut assemblies are commonly used in machines and structures to enable easy assembly and disassembly. However, the axial force (i.e. the fastening force) of such assemblies decreases due to recursive external loading on the bolt/nut assemblies or chronic progressive wearing of the assemblies. Consequently, axial force monitoring is essential in preventing serious failure due to loss of functions in the assembly or fatigue. This study proves that the axial force on bolt/nut assemblies can be measured by investigating changes in the bending mode natural frequency of the bolt's threaded portion that protrudes from the nut (hereinafter referred to as the "protruding thread part"). This method is postulated on the observation that a reduction in the axial force decreases the joint stiffness of the bolt/nut assembly at the protruding thread part, leading to a shift in the characteristic peak frequency of the bending mode. A bolt/nut assembly is formed and its bending mode shapes and bending mode frequencies are obtained by impact tests. A series of tests are performed to define a quantitative measure of the correlation between the shift in the bending mode frequency and the axial force on the bolt/nut assembly. This method enables to perform measurement of the axial force on the bolt/nut assembly of −40 to −50% in the frequency range between 25 and 35 kHz. Dependency of the accuracy of this method on bolt aspect ratio (protruding length/nominal diameter) shows that lower aspect ratios are better suited for measuring axial force via bending mode frequency variation.

1. Introduction

In typical machines and structures, bolts and nuts are used for easy assembly, disassembly, and maintenance. However, monitoring of axial force (namely, a fastening force) is critical because weakening of the axial force of bolt/nut assemblies may result in fatigue fractures due to the vibrations and chronic structural degradation. To assess these issues, (a) hammering tests, (b) torque tests, and (c) ultrasonic tests are currently used. The hammering tests is widely spread technique of common knowledge in which the experimenter listens to and evaluates the sound from an inspection target structure while hitting it with a hammer. In hammering tests, the assessment of the weakening torque of a bolt, bolt/nut assembly or bolted joint is often based on the tester's capability to discern the characteristic sound emitted by the vibrating units when tested individually. Traditional hammering tests can be used for bolts with almost no applied axial force, however, this kind of test does not provide a quantitative measure of the actual axial force. In addition, the test results are strongly depended on the tester's technical skills. Torque tests, which control the axis force using a calibrated wrench, are widely employed. This method can be easily conducted, but precisely evaluating the axial force is difficult because the frictional property of the screw seating surface varies according to the degree of fastening [1–3]. Several techniques based on ultrasonic testing exist; the ones most commonly employed entail measuring the latency in the acoustic propagation from the bolt head [4–7], the ratio between longitudinal and transverse wave velocity [8–12], combined vibration modes and longitudinal ultrasonic waves [13], electromechanical impedance monitoring [14], Lamb waves [15], or the shift in the resonant frequencies [16–18]. However, these methodologies are

* Corresponding author.
E-mail addresses: hosoya@sic.shibaura-it.ac.jp (N. Hosoya), md16062@shibaura-it.ac.jp (T. Niikura), hasimura@sic.shibaura-it.ac.jp (S. Hashimura), ikajiwara@eng.hokudai.ac.jp (I. Kajiwara), f.giorgio-serchi@ed.ac.uk (F. Giorgio-Serchi).

https://doi.org/10.1016/j.measurement.2020.107914
0263-2241/

still subject to large inaccuracies due to the multitude of factors which affect the estimation of the axial force.

To resolve such challenges, many approaches have been devised to assess the axial force on bolt/nut assemblies. State-of-the-art techniques entail the direct measurement of the axial force by means of sensors embedded in the bolt such as strain gauge, fiber grating sensor [19], and lead zirconate titanate (PZT) [20,21]. Additionally, a method that incorporates a thin plate sensor into bolt/nut assemblies has been considered [22–25]. These methods rely on the embedding of additional sensor nodes within the bolted joint or in contact with the bolt/nut unit. Other methods have eliminated the additional devices by using the same number of sensors as that of the bolt/nut assemblies in the intended structure to assess dynamic changes [26–29]. However, bolt status observations using this method are impractical because they require the embedding of electrical cables and a data logger apparatus to collect the data about the bolts and bolt/nut assemblies from a multitude of sensors. Furthermore, a method that uses the natural frequencies of the target structures with bolt/nut assemblies has been examined [25], but its efficacy is difficult to evaluate because of its dependency on the characteristics of the subject bodies. Alternative methods which use optical characteristics include the measurement of the strain on the washer side by a high-resolution CCD camera and an automated digital image correlation method [29] or via 3D electronic speckle pattern interferometry [30]. However, these approaches require dedicated space to accommodate the optical apparatus around the bolt/nut assemblies. Finally, a number of methodologies entail the measurement of the changes in the surface properties which occur at the interface between the bolt and the nut (i.e. change in contact area); some examples are contact acoustic nonlinearity, vibro-acoustic modulation, Recognition-Taguchi method and time reversal operation [31–37]. However, the output from such systems is negatively affected by the roughness of the surfaces between the subject bodies to be fastened.

As an alternative to the above mentioned techniques, this study proposes to derive the axial force of a bolt/nut assembly based on the correlation between the change in this axial force and the shift in the bending frequency mode of the protruding part of the bolt's threaded portion (hereinafter referred to as the "protruding thread part"). This method follows from the observation of Okugawa et al. [22], according to which a decrease in the axial force of a bolted joint caused the decrease of its joint stiffness which, in turn, manifested itself in the decrease of the characteristic natural frequency of the *smart washer*. Taking the cue from these observations, we assess the feasibility of estimating the axial force of a bolted joint based on the relationship between the variation in a local mode frequency of a bolt head and its clamping torque [38]. Our earlier work on this technique was affected by two issues. First, the evaluation of the axial force based on the clamping torque performed via a calibrated torque wrench is subject to loss of accuracy due to the friction at the thread and at the bearing surface. Secondly, it became apparent that, in order for this method to be applicable, rigorous criteria for the inference of axial force had to be defined.

Despite the results of [22], there has been no attempt in earlier works [1–37] to evaluate the axial force of bolt/nut assemblies via the characterization of the vibration mode frequency of the protruding threaded part. Hence, this work aims at defining a protocol to study the shift in the natural frequency of the bending mode of the protruding thread part of a bolted connection and use this data to infer the axial force acting on the bolt.

The experimental work presented here addresses three main aspects. First, it uses a widespread impact testing method to perform the experimental modal analysis. From this the relationship between axial force and variation in the bending mode frequency of the protruding threaded part of the bolt is derived. Here we employ the experimental modal analysis in the ultrasonic frequency range, because the highest frequencies are more prone to variation [32], thus enabling a more accurate measurement of the axial force. But the use of the term "ultrasonic" does not refer to the ultrasonic waves such as longitudinal or transverse waves. Rather, we use this term to specify the range of frequency of the experimental modal analysis within which we operate. Secondly, we expand on previous work by employing strain gauges embedded in the testing rig for accurate calibration of the axial force. This represents a significant improvement with respect to the use of calibrated torque wrench since this technique has been shown to be excessively sensitive to the frictional properties of the screw seating. Finally, the experiments reported here account for a broad range of axial force variations and numerous iterations of loosening and fastening. (Hereinafter the number of times of loosening and re-fastening is referred to as the "number of fastenings".) Estimates of the sensitivity to axial force measurement of this method to aspect ratio (protruding length/nominal diameter) of the bolt are also provided.

2. Experimental testbed: The bolt/nut assembly

The test bolts consisted of three common types of bolts in machines and structures: M8, M10, and M12. Fig. 1 shows the test bolts and the test nuts. Table 1 shows the sample bolt sizes. The length of the protruding thread part was defined as the aspect ratio, which is protruding length divided by nominal diameter d, and we tested for three values: 0.7, 1.7, or 3.7. The purpose of employing bolts with different aspect ratio is motivated by the need to assess the sensitivity of the measured axial force to the length of the protruding thread part and the bolt size. The broad variety and sizes of bolts make it necessary to estimate how the reliability of this measurement method varies when applied to bolt of different characteristics. For the test bolts, commercially available high-strength hexagon head bolts (property class: 10.9, material: carbon steel, coating: alkaline blackening) were employed. As

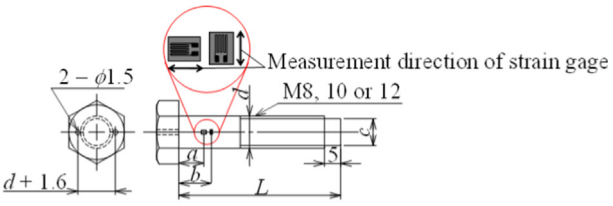

(a) Test bolts: A, B, D or E (aspect ratio 0.7 or 1.7).

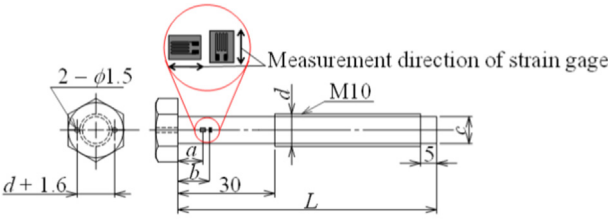

(b) Test bolt: C (aspect ratio 3.7).

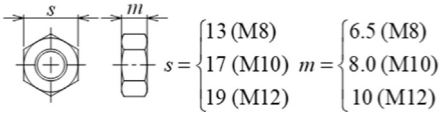

(c) Test nuts

Fig. 1. Test bolts and test nuts (see Table 1). (a) Test bolts: A, B, D, and E (aspect ratio: 0.7 or 1.7), (b) test bolt: C (aspect ratio: 3.7) and (c) test nuts.

Table 1
Specifications of the five test bolts.

Test bolt	Nominal diameter d [mm]	Property class	Nominal length L [mm]	Protruding length [mm]	Protruding diameter c [mm]	Aspect ratio	Position of the strain gauge [mm]	
							a	b
A	M10	10.9	49.7	6.7	8.4	0.7	15	20
B	M10	10.9	59.8	16.8	8.4	1.7	20	25
C	M10	10.9	80.2	37.2	8.4	3.7	20	25
D	M8	10.9	47.1	5.6	6.0	0.7	15	20
E	M12	10.9	53.4	8.4	9.6	0.7	10	15

shown in Fig. 1, the axial force was measured by four strain gauges (KFR-02-120-C1, Kyowa Electronic Instruments Co., Ltd., gauge length: 0.2 mm) that were attached to points just under the bolt head in the front and back of the bolt. For each point, two gauges were attached to measure the axial force along and across the axis. As anticipated, the employment of strain gauges in place of the calibrated torque wrench is motivated by the excessive dependency of this latter technique to frictional properties of the screw seating. The heads of test bolts were processed to have two through holes with 1.5-mm diameters for the cables of the strain gauges to pass.

To facilitate excitation to the protruding thread part by an impulse hammer, the screw thread was ground and 5 mm were removed from the tip. Due to thread rolling manufacturing processes, commercially available bolts of longer lengths have lower straightness of the threaded part. In this study, only for bolt C, which had a longer L than the others, the areas where the strain gauges were attached were ground to ensure that the straightness of the screws of bolt C were equivalent to the other bolts (Fig. 1(b)). The nominal axial force was defined to be 60% of the 0.2% proof stress of each bolt: 19.76 kN for M8, 31.32 kN for M10, and 45.52 kN for M12. This paper considers these values to be 100% of the nominal axial force.

For test nuts, commercially available hexagon nuts style 2 (double chamfer, material: carbon steel, coating: alkaline blackening) were used.

The strain gauges were calibrated to accurately measure the axial force. The load (axial force) was measured by a calibrated load cell (LCW-C-50KN50SA3, Kyowa Electronic Instruments Co., Ltd.) and the strain was measured by a strain gauge attached to the test bolt to establish the relationship between the axial force and the strain. The number of fastenings (the number of trials in the axial force calibration tests) was 10. Identical conditions were used for each calibration test.

Fig. 2 shows the bolt/nut assembly used in this experiment. The subject body was a single-piece cube made of medium carbon steel

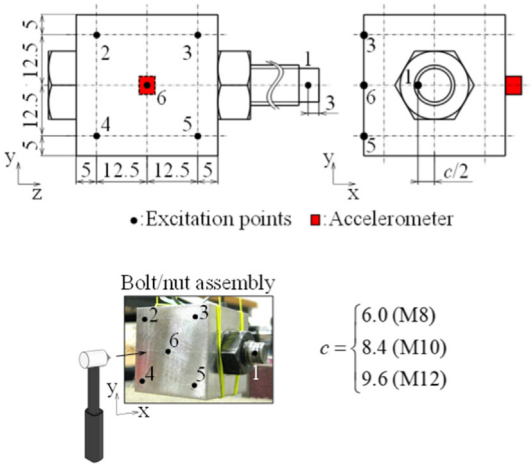

Fig. 2. Bolt/nut assembly.

(C50) with 35-mm sides to eliminate the influences due to friction between multiple subject bodies and those from the natural frequencies or the vibration modes of the subject bodies on the accuracy of the assessed axial force. A through hole was made through the center of the cube and a bolt was fastened through this hole. Three types of cubes were made to accommodate the three types of test bolts used in this experiment (M8, M10, and M12). The diameters of the through holes were 9 mm for M8, 11 mm for M10, and 13.5 mm for M12. When fastening the test bolts, a bolt tension stabilizer (Fcon, Tohnichi Manufacturing Co., Ltd., density: 0.89 g/cm^3 at 20 °C, viscosity: approx. 15000 mPa·s at 24 °C) was applied to the screw thread surface of the bolt and to the bearing surface of the nut to suppress variations in the friction factors to achieve sustainable fastening.

We used a single-piece cube (35-mm sides) made of carbon steel (C50) as the subject body to be fastened. In the first stage of this study, we eliminated the impact from the friction between multiple subject bodies and those from the natural frequencies or vibration modes of the subject bodies. This was motivated by the need to conduct a laboratory test in the simplest possible configuration in order to reliably establish the relationship between the decreased axial force and the decreased bending mode natural frequency of the protruding thread part.

3. Vibration testing

3.1. Measurement of the frequency response functions

For the bolt/nut assembly shown in Fig. 2, the natural frequencies and the vibration mode shapes of its protruding thread part were determined by conducting an impact test using an impulse hammer. There were six excitation points. Point 1 was on the protruding thread part and Points 2–6 were on the cube surface. Each point was excited in sequence using an impulse hammer (Type 8204, Brüel & Kjær Sound & Vibration Measurement A/S, sensitivity: 22.26 mV/N) and the responses were measured using an accelerometer attached directly behind Point 6 (352C15, PCB Inc., sensitivity: 0.973 mV/(m/s^2), mass: 2 g, natural frequency: 50 kHz or higher) and recorded by a spectrum analyzer (A/D: NI PXI-4472B, National Instruments Co., Software: CAT-System, CATEC Inc.). From the relationship between these inputs and outputs, six frequency response functions (FRFs) were measured. The bolt/nut assembly was suspended using a thin string to make it free of support. The number of fastenings was ten and the average count (the number of hits by the impulse hammer) for one identical fastened state was also ten. For the measurement, the number of sampling points, the sampling frequency, and the measurable frequency were 32,768, 102.4 kHz, and 40 kHz, respectively.

3.2. Finite element analysis

As far the experimental analysis is concerned, a difficulty arises with the detection of those modes associated with the vibration of

the bolt within the subject body. In order to achieve a description of these specific modes despite the lack of experimental data, we resorted to finite element analysis, as reported in Fig. 5(a) and (b). Previous work on this matter [22] has shown to not be suitable, in this respect. Hence, differently from [22], we implement the finite element model with solid elements in order to examine the mode shapes within the subject body. Our previous work based on the use of solid elements in the frame of bolt loosening analysis [32] examined the change in contact areas between the seating surfaces of the bolt head/nut corresponding to a change in the axial force in the bolt/nut assemblies. Within the remit of the current manuscript, our objective is not to develop an advanced finite element model to assess axial force in bolt/nut assemblies, but merely to highlight that a finite element model which accounts for nominal axial force can be produced if bonded and contact (friction) elements are properly incorporated.

Our starting assumption is that a change in the rigidity of the fixed end corresponds to a change in the axial force of the bolt/nut assembly. An analogous assumption has been successfully established in the work of [22], referred to as the *smart washer* case, which we briefly review here for reader's convenience. A critical distinction between our work and that of [22], however, lies in the axial force not being evaluated directly in [22]. Indeed, in [22], the frequency equation reads,

$$
\begin{aligned}
&(\sin\beta l+\sinh\beta l)\Omega_1-(\cos\beta l+\cosh\beta l)\Omega_2+2\Omega_3=0\\
&\Omega_1=2\frac{EI\beta}{k_R}\cos\beta l-\sin\beta l+\sinh\beta l+\frac{(EI\beta^2)^2}{k_Tk_R}(\sin\beta l+\sinh\beta l)\\
&\Omega_2=\left\{1+\frac{(EI\beta^2)^2}{k_Tk_R}\right\}\left(2\frac{EI\beta}{k_R}\sin\beta l+\cosh\beta l+\cos\beta l\right)\\
&\Omega_3=\frac{EI\beta^3}{k_T}\left\{\left(\cos\beta l+\frac{EI\beta}{k_R}\sin\beta l\right)\left(\frac{EI\beta}{k_R}\cos\beta l+\sinh\beta l\right)\right.\\
&\qquad\left.+\left(\sin\beta l-\frac{EI\beta}{k_R}\cos\beta l\right)\left(\frac{EI\beta}{k_R}\sin\beta l+\cosh\beta l\right)\right\}\\
&\beta^4=\frac{\rho A\omega^2}{EI}
\end{aligned}
\tag{1}
$$

where l, E, I, A, ρ, ω, k_T and k_R are the length of the cantilever, Young's modulus, the moment of inertia of cross section, the cross-section area, the density, the angular frequency, the translational spring constant and the rotational spring constant at the cantilever fixed end, respectively. According to [22], Eq. (1) confirms the occurrence of the correlation between axial force variation (corresponding to the rigidity of the end) and a shift in the bending modes frequency. Certainly, a Timoshenko beam model might be better suited to estimate the effect on stiffness of the protruding thread part with translational and rotational springs. However, the correlation between a cantilever's (smart washer's) natural frequency and an axial force is better highlighted based on numerical results from this simple model [22].

For finite element analysis (FEA), the solver, the element type, the number of nodes, and the number of elements were ANSYS15.0, Solid185, 62,690, and 55,738, respectively. The element size was 0.5 mm for a screw surface and 1 mm for the other areas. The contact conditions between the bolt and nut seat surface and the subject body were set to bond. In this case, this finite element model did not consider the preload to the bolted joint. We have just analyzed using bonded element. In general, it is hard to make a precise finite element model with preload to bolted joints. Similarly, the contact conditions between the threaded surfaces of the bolt and nut were set with friction (friction coefficient: 0.2, contact surface: bolt side surface (Conta173), target surface: nut internal surface (Targe170)). The thread surfaces were reproduced by initially modeling as a cylinder with ϕ10 and then providing a modeled cylinder with standard values of a M10 bolt (mean pitch diameter, 9.026 mm; distance between pitches, 1.5 mm; and thread angle, 60°) virtually using the geometry correction function. The material property of the subject body, bolt, and nut was set to steel for a general structure (Young's modulus: 200 GPa, density: 7,850 kg/m^3, and Poisson's ratio: 0.3). The modal damping ratio to determine the FRFs with FEA was set to 0.04–0.13%. The modal damping ratios were empirically estimated by fitting the calculated FRFs by FEA with those obtained by the experiment.

3.3. Natural frequencies and vibration mode shapes

Bolt A was screwed to the bolt/nut assembly at the nominal axial force of 31 kN (100%). Fig. 3 shows a representative time history of the wave shape measured when Point 1 was excited, while Fig. 4 shows the averaged cross-FRF (H_{61}) of Point 6–1. Fig. 4 also shows the coherence function, the phase characteristics, and the amplitude of the FRF. For comparison, the FRF obtained by FEA is overlaid.

We used both the experimental modal analysis and FEA to identify which natural frequencies are bending mode shapes. Fig. 3 shows that the vibration response as a function of time of the bolt/nut assembly damps in about 5 ms. The FRF obtained in this experiment agrees well with the FRF obtained by FEA (Fig. 4). In addition, four natural frequencies (two near 20 kHz and two near 35 kHz) are revealed within the frequency range in this experiment consistent with the fact that the bolt/nut assembly has repeated roots. Subsequently, based on the six FRFs, the modal parameters (natural frequencies, mode shapes, etc.) were identified.

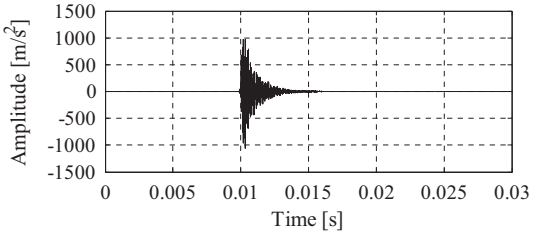

Fig. 3. Measured time response of the bolt/nut assembly of a test bolt: A (size: M10, aspect ratio: 0.7, axial force: 31 kN = 100%).

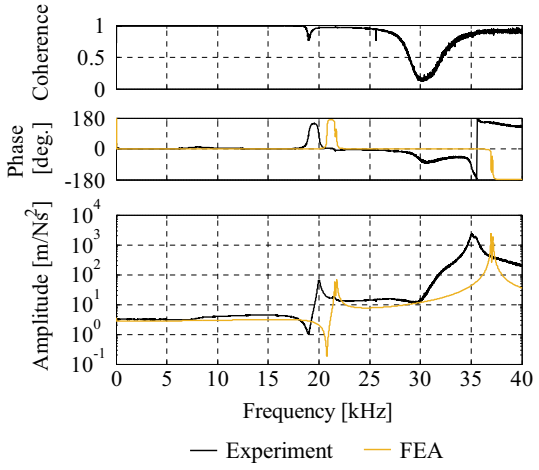

Fig. 4. Coherence function, phase characteristics, and amplitude of the cross-frequency response function (FRF) (H_{61}) measured by impulse testing (black line) and those obtained by finite element analysis (FEA) (orange line) of the test bolt: A (size: M10, axial force: 31 kN = 100%). (For interpretation of the references to colour in this figure legend, the reader is referred to the web version of this article.)

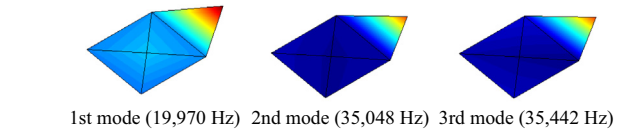

(a) Impact testing (axial force: 31 kN = 100%).

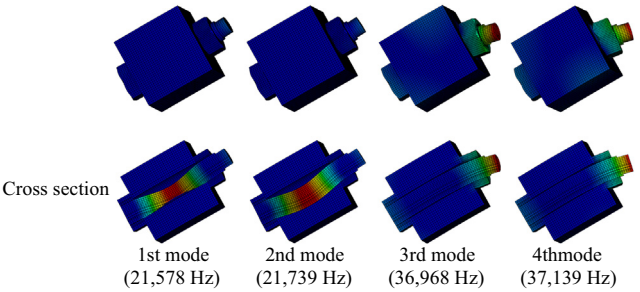

(b) Finite element analysis.

Fig. 5. Vibration mode shapes of the bolt/nut assembly of the test bolt: A (size: M10, aspect ratio: 0.7). (a) Impact testing (axial force: 31 kN = 100%) and (b) finite element analysis.

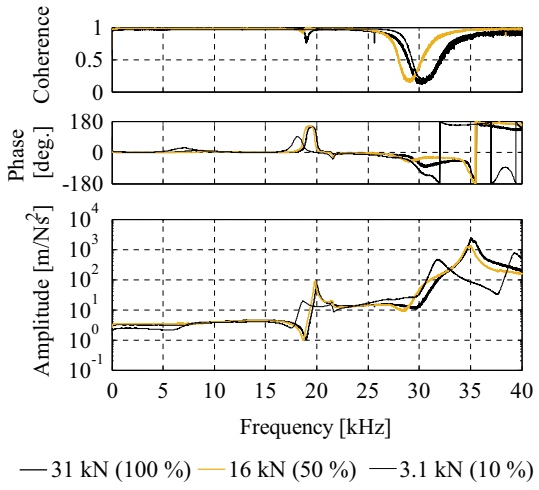

Fig. 6. Measured coherence function, phase characteristics, and amplitude of the cross- frequency response function (FRF) (H_{61}) by changing the axial force of 31 kN (100%) (black line), 16 kN (50%) (orange line) and 3.1 kN (10%) (thin black line) of the test bolt: A (size: M10, aspect ratio: 0.7). (For interpretation of the references to colour in this figure legend, the reader is referred to the web version of this article.)

Figs. 5(a) and (b) show the vibration mode shapes obtained from the experiment and FEA, respectively. In Fig. 5(b), the sectional view of the test bolt along its center axis is shown as a reference. Based on Figs. 4 and 5, the percentage difference between the natural frequencies measured from the FRFs is about 5% and the mode shapes agree with each other. In addition, the vibration mode of the protruding thread part has repeated roots, including the bending mode where the subject body does not vibrate and only the protruding thread part vibrates. In this paper, the lower and higher natural frequencies of the bending mode of the protruding thread part are respectively defined as the primary and secondary modes. A target measurement direction in the experimental modal analysis was set to x axis with acceleration (see Fig. 2). As shown in the 2nd mode or 3rd mode of Fig. 5(a), in the case where the vibration mode shape displayed an angle between the vibration direction of the bending mode and the x axis, and both modes along the x axis exist, it is not possible to distinguish between these modes. These modes might be corresponding to the 3rd mode or the 4th mode of Fig. 5(b), respectively.

The vibration mode near 20 kHz for the FRF in Fig. 4 and for the vibration mode shape in Fig. 5 were analyzed by experimental modal analysis and FEA. A vibration mode where the bolt vibrates within the subject body is observed in Fig. 5(a) and (b). This mode also has repeated roots. But the experimental modal analysis could not visualize this repeated roots. Based on these results, an impact test can clarify the natural frequencies and vibration modes of the bending mode of the protruding thread part. In our method, an identification of the bending mode frequency of the bolt/nut assembly is important, because we measure the axial force of the bolt/nut assembly using this relationship between the bending frequency of the protruding thread part and the axial force. In the next section, we investigate the relationship between them.

3.4. Axial force measurement

The starting point of this analysis consists in confirming whether a change in the bending mode frequency of the protruding thread part is correlated to a change in the axial force of the bolt/nut assembly. Fig. 6 shows the cross-FRFs at Points 6–1 for bolt A. The FRFs measured with the axial forces of 31 kN (100%), 16 kN (50%), and 3.1 kN (10%) are overlaid for comparison. The coherence function, the phase characteristics, and the amplitude of the cross-FRF are also shown. It is apparent from these results that the bending mode frequency decreases as the axial force decreases, in agreement with previous observations [22,26,28,32]. It is also observed that the bending mode frequency is more sensitive to the axial force variation than the mode frequency within the subject body around 20 kHz (see Fig. 6).

Having ascertain the existence of a clear correlation between axial force variation and shift in the bending modes frequency, we devise a methodology to quantify accurately the variation in axial force by focusing exclusively on the frequency response of the protruding thread part. To do so, we first need to record the frequency variation at fine decrement of the axial force. This will be needed to define threshold criteria which enables to capture unambiguously the loosening effect.

Hence the FRFs were measured while the axial force was decreased incrementally in 10% steps from the nominal value of 31 kN (100%) to 3.1 kN (10%). Fig. 7 shows the relationship between the axial force and the bending mode of bolt A. Both the primary and the secondary bending mode frequencies during 10 fastenings are overlaid. The bending mode frequency decreases as the axial force decreases, which agrees with previous studies [22,26,28,32]. Additionally, there are some variations in the bending mode frequency measured for each fastening. To measure the axial force of the bolt/nut assembly based on the relationship between the bending frequency of the protruding thread part and the axial force, a threshold is needed. In this paper, we decide the threshold considering a variation of the bending mode

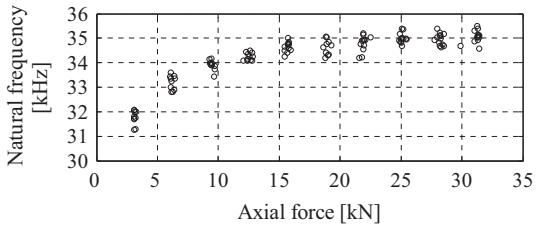

Fig. 7. Relationship between the measured bending mode frequency of the protruding thread part and the axial force of test bolt: A (size: M10, aspect ratio: 0.7).

frequency during 10 fastenings. Furthermore, when the threshold is decided, the primary and the secondary bending mode frequencies are undistinguished. The change rate of the bending mode frequency is given by

$$CR_i = \frac{(f_i - f_n)}{f_n} \times 100\ \% \tag{2}$$

where CR is the change rate, f_n is the mean bending mode frequency under the nominal axial force, f_i is the mean bending mode frequency measured at each axial force, subscript i is the number of axial force trials.

Fig. 8 shows the relationship between the change rate of the bending mode frequency and the axial force corresponding to Fig. 7. The black triangles represent the mean of the bending mode frequencies measured in the ten fastenings, while the error bars denote the coefficients of variation in the bending mode frequency that is defined as

$$CV_i = \frac{\sqrt{\frac{1}{p-1}\sum_{j=1}^{p}\left(\tilde{f}_j - f_i\right)^2}}{f_i} \times 100\% \tag{3}$$

where $\tilde{f}_j$ is each bending mode frequency measured at each axial force and p is the number of bending mode frequency at each axial force. In Fig. 8, the mean bending mode frequency measured at each axial force is normalized using the mean bending mode frequency under the nominal axial force of 31 kN (100%). Using Eq. (3), we obtain CV of the bending mode frequency under the nominal axial force is 0.8%. (See (4) of Fig. 9.)

This study measures the axial force using the following procedure (Fig. 9).

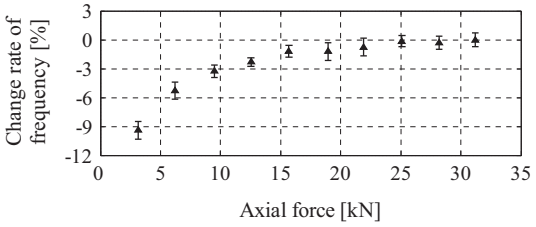

Fig. 8. Relationship between the change rate of the bending mode frequency of the protruding thread part and the axial force of the test bolt: Corresponding to Fig. 7 (size: M10, aspect ratio: 0.7).

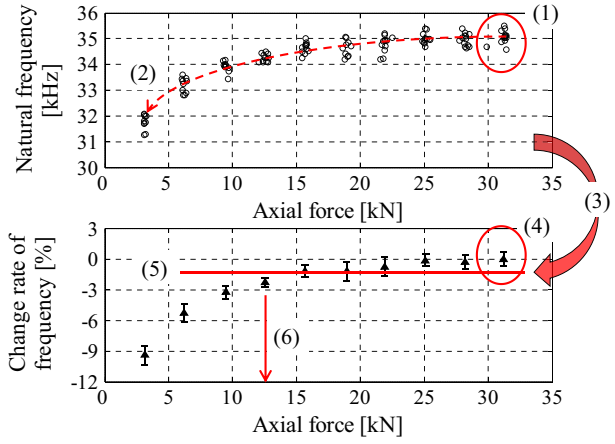

Fig. 9. Procedure of determination of an axial force of a bolt/nut assembly.

(1) The bending mode frequency is measured with a nominal axial force and number of fastenings.
(2) The bending mode frequency with the nominal axial force and that with a decreased axial force are compared.
(3) The change rate of the bending mode frequency is derived.
(4) The coefficient of variation of bending mode frequencies of the protruding thread part is investigated using the nominal axial force. When we obtain the coefficient of variation, bolt/nut assemblies are loosened and refastened multiple times, allowing variations in the degree of fastening and axial force to be considered. The coefficient of variation also includes the difference of the bending mode frequencies between the primary and the secondary bending mode frequencies (repeated roots).
(5) A threshold is decided considering the coefficient of variation of bending mode frequencies with the nominal axial force.
(6) The point where the bending mode frequency exceeded the threshold, which is defined using the coefficient of variation of the bending mode frequency, is determined. The axial force is measured by systematically decreasing the axial force from the nominal one.

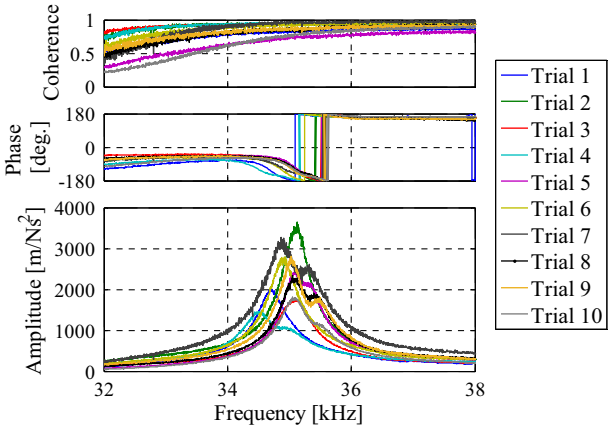

Fig. 10. Variation of the bending mode frequency during ten fastenings of the test bolt: A (size: M10, aspect ratio: 0.7).

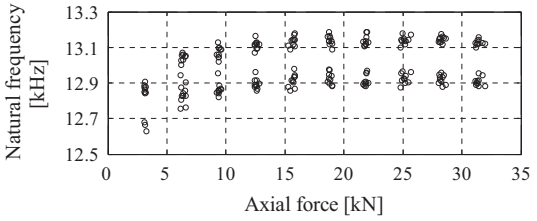

(a) Test bolt: B (size: M10, aspect ratio: 1.7).

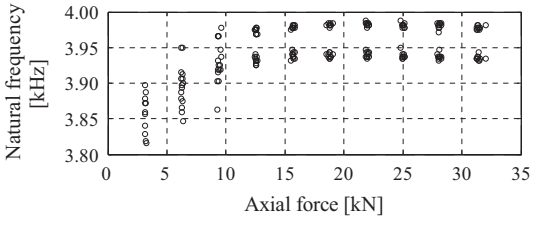

(b) Test bolt: C (size: M10, aspect ratio: 3.7).

Fig. 11. Relationship between the measured bending mode frequency of the protruding thread part and the axial force. (a) Test bolt: B (size: M10, aspect ratio: 1.7) and (b) test bolt: C (size: M10, aspect ratio: 3.7).

In this study, the axial force is determined as 13 kN (40%) by setting the threshold as the point where the frequency decreased by 0.8% or more. This value (0.8%) is the *CV* of the bending mode frequency under the nominal axial force.

3.5. Accuracy of axial force detection

3.5.1. Variation of the bending mode frequency

For bolt A, factors that generate variations in the bending mode frequency of the protruding thread part were investigated. Fig. 10 shows a magnified image of the cross-FRF (H_{61}) near 35 kHz (natural frequency of the bending mode of the protruding thread part) observed with the nominal axial force of 31 kN (100%). The FRFs measurement from data acquired after ten fastenings are overlaid for comparison as well as the coherence function, the phase characteristics, and the amplitude of the cross-FRF. As shown in Fig. 10, in three fastening trials, both of the repeated roots (the primary and the secondary bending mode frequencies) can be found. However, only one root can be found in the remaining seven trials. These ten trials are the same experimental conditions.

3.5.2. Treatment of the repeated root

Subsequently, for bolts B and C, which differ from A only with respect to the aspect ratio, factors that generate variations in the natural frequency of the bending mode of the protruding thread part were investigated. Fig. 11 shows the relationship between the axial force and the bending mode frequency in bolts B and C. In every fastening trial, when the aspect ratio is changed, both of the repeated roots can be found except for the following axial force conditions: the axial force of 3.1 kN (10%) and 6.2 kN (20%) in bolt B and the axial force of 3.1 kN (10%), 6.2 kN (20%) and 9.4 kN (30%) in bolt C.

Slight variation in the values of axial force during the 10 identical repetitions is attributed to the fact that the axial force is set manual. Hence our method is designed to disregard minor variations while capturing the more significant effect in the frequency

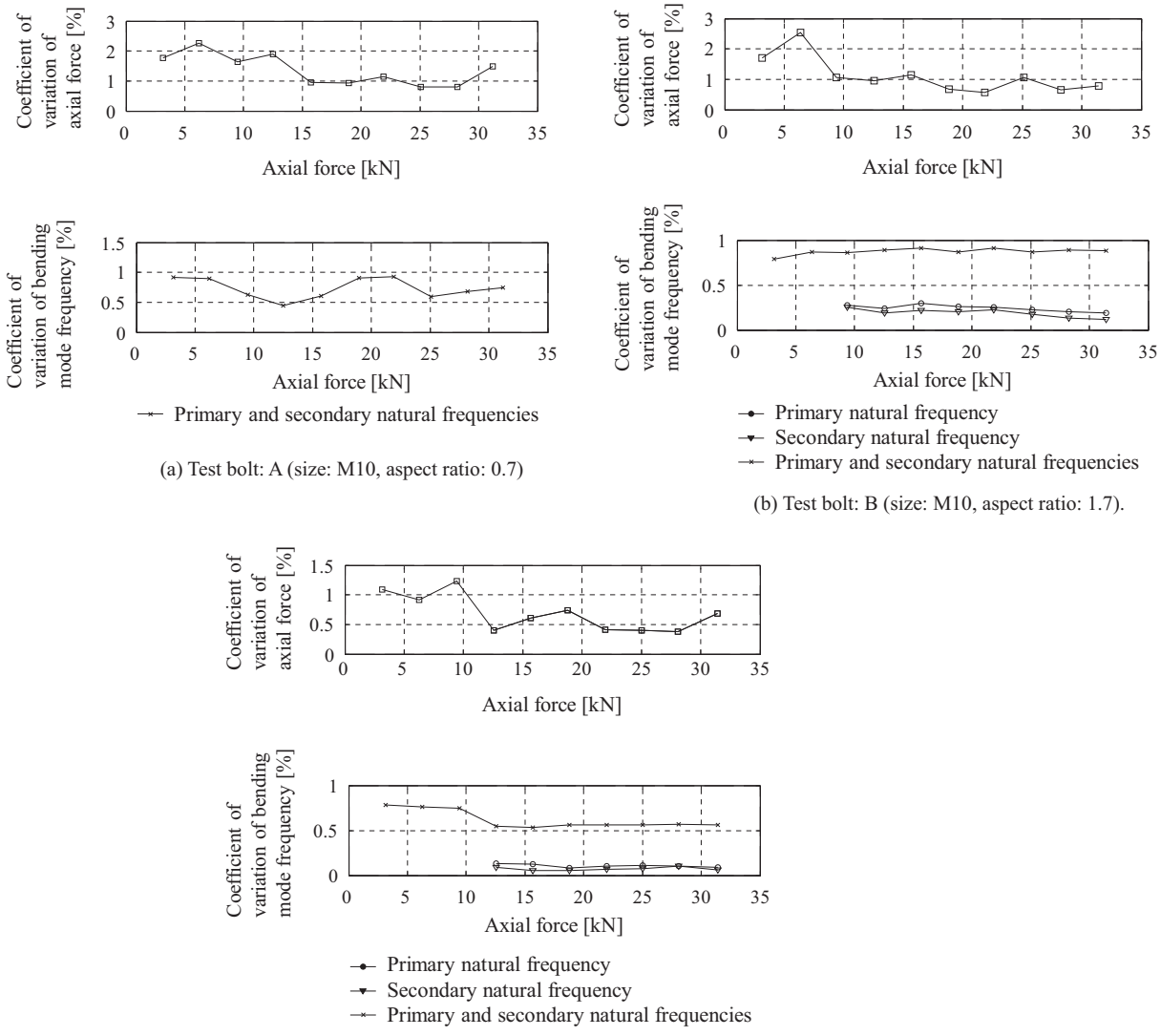

(a) Test bolt: A (size: M10, aspect ratio: 0.7)

(b) Test bolt: B (size: M10, aspect ratio: 1.7).

(c) Test bolt: C (size: M10, aspect ratio: 3.7).

Fig. 12. Relationship between the coefficient of variation and the axial force for three test bolts. (a) Test bolt: A (size: M10, aspect ratio: 0.7), (b) test bolt: B (size: M10, aspect ratio: 1.7) and (c) test bolt: C (size: M10, aspect ratio: 3.7).

shift attributed to actual changes in the axial force. Fig. 12(a) to (c) show the coefficients of variation of the axial force and the coefficients of variation bending mode frequency at each setting axial force (10–100%), respectively. The lower of Fig. 12(a) to (c) correspond to Figs. 8 and 11, respectively. In Fig. 12(a), the primary and the secondary modes cannot be differentiated because both modes do not almost always exist. Fig. 12(b) and (c) present the coefficients of variation obtained with and without differentiation of the primary and the secondary modes for comparison. The coefficients of variation of the primary and the secondary modes results in a 0.1% variation of the coefficients for both bolt B and C, respectively. In contrast, the variation of the coefficients of the bending mode frequency is about 0.8% for bolt A, 0.9% for bolt B and 0.6% for bolt C without differentiation of the primary and the secondary modes (with the nominal axial force). In addition, the coefficient of variation of the bending mode frequency is smaller than that of the axial force (see Fig. 12). The coefficient of variation of the axial force is about 1.5% for bolt A, 0.8% for bolt B and 0.7% for bolt C with the nominal axial force, respectively. The coefficient of variation of the axial force is larger than the coefficient of variation of the primary and the secondary modes. Based on these results, the variation in the bending mode frequency is attributed to the difference between the primary and secondary bending mode frequencies. Meanwhile the variation of each axial force during 10 fastenings or random errors in measurements do not largely affect the variation of the bending mode frequency.

The fact that both the primary and secondary modes can be found in some cases but only one can be found in others may be due to the change in the fastening state of the bolt and nut, which is affected by complex factors, including lubrication and friction. Therefore, the proposed axial force measurement method using the bending mode frequency of the protruding thread part while considering variations of repeated roots' frequencies without differentiating the primary and secondary frequencies is efficient, allowing a usability procedure. In the following section, the coefficient of variation of the bending mode frequencies is determined without differentiating the primary and secondary modes.

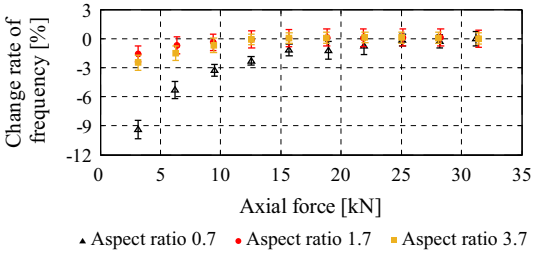

Fig. 13. Relationship between the change rate of the bending mode frequency of the protruding thread part and axial force for the three aspect ratios of the test bolts (corresponding to Figs. 8 and 11).

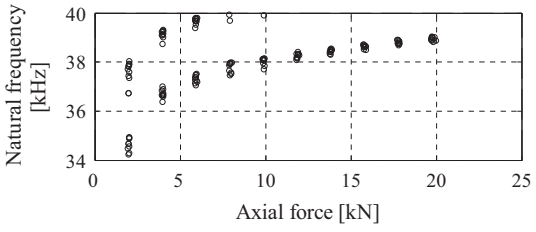

Fig. 14. Relationship between the measured bending mode frequency of the protruding thread part and the axial force of test bolt: D (size: M8, aspect ratio: 0.7).

3.5.3. Effect of aspect ratio of the protruding thread part in axial force detection performance

The impact of the length of the protruding thread part on the accuracy of the axial force assessment was also investigated. Fig. 13 shows the relationship between the axial force obtained by the procedures described in Section 3.4 and the change rate of the natural frequency, corresponding to Fig. 11(a) (bolt B) and Fig. 11(b) (bolt C). For comparison, the results shown in Fig. 8 for bolt A are overlaid. Considering the coefficients of variation for bolts B and C, an axial force assessment was performed, yielding axial forces of approximately 3.0 kN (≅10%) for bolt B and 6.3 kN (20%) for bolt C. Based on these results, an aspect ratio of 0.7 provides a better accuracy of the axial force assessment within the range accounted for in this study as the axial force of bolt A is assessed as 13 kN (40%). This result is of importance in the prospect of using this methodology in real-world applications, demonstrating that in order to employ this technique, we must be able to define an optimal length of the protruding part.

3.6. Applicable range

The accuracy of the axial force assessment was examined using M8 (bolt D) and M12 (bolt E). Based on the insight obtained in Sections 3.4 and 3.5, the aspect ratio was set to 0.7. Figs. 14 and 15 show the relationships between the axial force obtained by the procedures described in Sections 3.4 and 3.5 and the bending mode frequency of the protruding thread part.

Fig. 14 (bolt D) shows that the measurement is not properly performed because in the range of the axial force from 20 kN (100%) to 10 kN (50%), the secondary mode exceeds 40 kHz, which is the upper limit of the measurement range. The frequency can be enhanced beyond 40 kHz to assess the axial force of bolt D. However, in typical impact tests, creating an excitation force in the high frequency band beyond 40 kHz is difficult. One solution may be to employ laser excitation technology [39–48] or spherical projectile impact method [49], but this needs to be further examined.

Fig. 15(a) (bolt E) shows that the primary and secondary natural frequencies (repeated roots) are successfully measured at every value of the axial force. Fig. 15(b) shows the relationship between the axial force obtained by the procedures described in Sections 3.4 and 3.5 and the change rate of the natural frequency, corresponding to Fig. 15(a). Fig. 15(b) implies that the coefficient

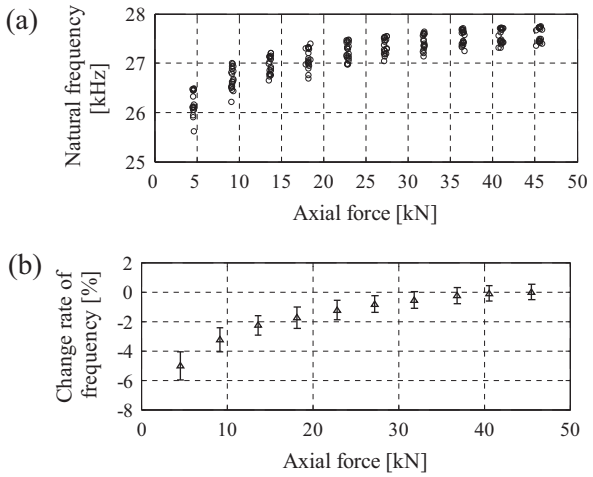

Fig. 15. Axial force assessment of the test bolt: E (size: M12, aspect ratio: 0.7). (a) Relationship between the measured bending mode frequency of the protruding thread part and the axial force and (b) the relationship between the change rate of the bending mode frequency of the protruding thread part and the axial force corresponding to (a).

of variation of the bending mode frequency for bolt E with the nominal axial force is approximately 0.5%. Taking this coefficient into account, the axial force is assessed to be 23 kN (50%) when the threshold is set in the same manner as described in Sections 3.4 and 3.5.

4. Conclusions

This study proves that it is possible to measure the axial force on bolt/nut assemblies by investigating the relationship between the bending mode natural frequency of the protruding thread part and the axial force. The results presented here demonstrate that it is feasible to perform contactless measurement of the fastening force of bolt/nut assemblies with remarkable accuracy, paving the way to the application of this methodology in real-world scenarios.

This experiment employed three types of high strength hexagon-head bolts, which are commonly used in general mechanical structures (M8, M10, and M12). In addition, the impact of length of the protruding thread part on the accuracy of axial force assessment was investigated by defining the length as the aspect ratio. Three ratios were examined: 0.7, 1.7, and 3.7. For M10 (aspect ratio 0.7), this method estimates its axial force to be 13 kN (40%) and for M12 (aspect ratio 0.7), the assessed axial force is 23 kN (50%). In general, a calibrated torque wrench has variations in measured axial force of ±30−±50% [2,3], while this method can accurately measure the axial force within −40 to −50% against the nominal axial force. This implies that if this method is to be used in real-world scenarios, then structural failure of the bolt/nut assemblies is extremely unlikely (i.e. operational conditions systematically lie below the yield stress), since this represents an underestimate at best.

By using impulse hammer testing along with FEA modeling we bring evidence of the occurrence of a strong correlation between axial force variation and natural frequency of the bolt/nut assembly. This is motivated by the protruding threaded part of the bolt and its axial force variation being assimilated respectively to a cantilever and a change in the rigidity of the cantilever fixed end.

We provide a new protocol which enables to effectively derive the axial force from the bending mode frequency response. This protocol is postulated on the definition of a coefficient of variation which allows to highlight meaningful divergence of the characteristic natural frequencies from a reference state (i.e. the nominal axial force) while at the same time filtering out random, small magnitude fluctuations in the fastening force.

The experiments bring evidence that the variation in the natural frequency which enables this methodology to be so effective relies on the difference between the primary and secondary natural frequencies, which exist due to the bending mode having repeated roots. Therefore, to realize an efficient and usability method, we should not distinguish the bending mode frequency of the protruding thread part of the primary and secondary frequencies. In addition, it is shown that the aspect ratio of the bolts does affect the accuracy of this method and that improved precision occurs for bolts with an aspect ratio of 0.7.

Finally, we show that the range of application of the proposed method is constrained to bolt sizes whose characteristic frequencies lie below the 40 kHz, i.e. to M8 bolts. This constraint, however, is solely attributed to the frequency excitation range enabled by impact tests and hence it is straight forward to overcome this limitation by employing more advanced technologies [39–49] such as laser-based or spherical projectile impact excitation which naturally operate on the high-frequency range.

Combined with laser excitation and laser Doppler vibrometer, our methodology has the potential to dramatically reduce the number of sensors and for the first time enabling automated, contactless fastening force estimation. In the near future, the impacts of the subject body (real assemblies with many modes or higher frequencies, material of bolted joints, surface roughness, thickness, the number of plates fastened, and the length of grip) and bolt material on the accuracy of the axial force assessment should be examined.

CRediT authorship contribution statement

Naoki Hosoya: Conceptualization, Methodology, Validation, Formal analysis, Investigation, Resources, Data curation, Writing - original draft, Writing - review & editing, Supervision, Project administration, Funding acquisition. **Takanori Niikura:** Methodology, Software, Validation, Formal analysis, Investigation, Resources, Data curation, Writing - original draft, Visualization. **Shinji Hashimura:** Validation, Resources, Writing - review & editing. **Itsuro Kajiwara:** Validation, Writing - review & editing. **Francesco Giorgio-Serchi:** Validation, Writing - review & editing.

Declaration of conflicting interests

The authors certify that there is no conflict of interest with the Precise Measurement Technology Promotion Foundation (PMTP-F) and the Japan Society for the Promotion of Science.

Acknowledgements

We thank the Precise Measurement Technology Promotion Foundation (Project No. 1-25) and the Japan Society for the Promotion of Science for support under Grants-in-Aid for Scientific Research programs (Grant-in-Aid for Challenging Exploratory Research, Project No. JP17K18858, and Grant-in-Aid for Scientific Research (B), Project No. JP19H02088).

References

[1] Y. Jiang, J. Chang, C. Lee, An experimental study of the torque-tension relationship for bolted joints, Int. J. Mater. Prod. Tec. 16 (2001) 417–429, https://doi.org/10.1504/IJMPT.2001.001264.
[2] X. Zhang, X. Wang, Y. Luo, An improved torque method for preload control in precision assembly of miniature bolt, J. Mech. Eng. 58 (2012) 578–586, https://doi.org/10.5545/sv-jme.2012.538.
[3] G.R. Toth, Controlled tightening over the yield point of a screw: based on Taylor's series expansions, J. Pressure Vessel Technol. 125 (2003) 460–466, https://doi.org/10.1115/1.1613299.
[4] H.J. McFaul, An ultrasonic device to measure high-strength bolt preloading, Mater. Eval. 32 (1974) 244–248.
[5] M. Suda, Y. Hasuo, A. Kanaya, Y. Ogura, T. Takishita, Y. Suzuki, Development of ultrasonic axial bolting force inspection system for turbine bolts in thermal power plants, JSME Int. J. I-Solid M. 35 (1992) 216–219, https://doi.org/10.1299/jsmea1988.35.2_216.
[6] A. Koshti, Ultrasonic measurement of the bending of a bolt in a shear joint, Exp. Mech. 38 (1998) 270–277, https://doi.org/10.1007/BF02410389.
[7] K. Jhang, H. Quan, J. Ha, N. Kim, Estimation of clamping force in high-tension bolts through ultrasonic velocity measurement, Ultrasonics 44 (2006) e1339–e1342, https://doi.org/10.1016/j.ultras.2006.05.190.
[8] G.C. Johnson, A.C. Holt, B. Cunningham, An ultrasonic method for determining axial stress in bolts, J. Test. Eval. 14 (1986) 253–259, https://doi.org/10.1520/JTE10337J.
[9] H. Yasui, H. Tanaka, I. Fujii, K. Kawashima, Ultrasonic measurement of axial stress in short bolts with consideration of nonlinear deformation, JSME Int. A-Mech. M. 42 (1999) 111–118, https://doi.org/10.1299/jsmea.42.111.
[10] S. Chaki, G. Corneloup, I. Lillamand, H. Walasxek, Combination of longitudinal and transverse ultrasonic waves for in situ control of the tightening of bolts, J. Pressure Vessel Technol. 129 (2007) 383–390, https://doi.org/10.1115/1.2748821.
[11] N. Kim, M. Hong, Measurement of axial stress using mode-converted ultrasound, NDT & E Int. 24 (2009) 164–169, https://doi.org/10.1016/j.ndteint.2008.09.005.
[12] X. Ding, X. Wu, Y. Wang, Bolt axial stress measurement based on a mode-converted ultrasound method using an electromagnetic acoustic transducer, Ultrasonics 54 (2014) 914–920, https://doi.org/10.1016/j.ultras.2013.11.003.

[13] B. Blachowski, A. Swiercz, P. Gutkiewicz, J. Szelążek, W. Gutkowski, Structural damage detectability using modal and ultrasonic approaches, Measurement 85 (2016) 210–221, https://doi.org/10.1016/j.measurement.2016.02.033.
[14] T.-C. Huynh, N.-L. Dang, J.-T. Kim, Preload monitoring in bolted connection using piezoelectric-based smart interface, Sensors 18 (2018) 2766, https://doi.org/10.3390/s18092766.
[15] R. Kędra, M. Rucka, Preload monitoring in a bolted joint using Lamb wave energy, Bull. Pol. Acad. Sci.-Te. 67 (2019) 1161–1169, https://doi.org/10.24425/bpasts.2019.131570.
[16] J.S. Heyman, A CW ultrasonic bolt-strain monitor, Exp. Mech. 17 (1977) 183–187, https://doi.org/10.1007/BF02330995.
[17] S.G. Joshi, R.G. Pathare, Ultrasonic instrument for measuring bolt stress, Ultrasonics 22 (1984) 270–274, https://doi.org/10.1016/0041-624X(84)90043-X.
[18] M. Hirao, H. Ogi, H. Yasui, Contactless measurement of bolt axial stress using a shear-wave electromagnetic acoustic transducer, NDT & E Int. 34 (2001) 179–183, https://doi.org/10.1016/S0963-8695(00)00055-4.
[19] A. Khomenko, E.G. Koricho, M. Haq, G.L. Cloud, Bolt tension monitoring with reusable fiber Bragg-grating sensors, J. Strain Anal. Eng. 51 (2016) 101–108, https://doi.org/10.1177/0309324715598265.
[20] S. Ritdumrongkul, Y. Fujino, Identification of the location and level of damage in multiple-bolted-joint structures by PZT actuator-sensors, J. Struct. Eng.-ASCE 132 (2006) 304–311, https://doi.org/10.1061/(ASCE)0733-9445(2006)132: 2(304).
[21] J. Shao, T. Wang, H. Yin, D. Yang, Y. Li, Bolt looseness detection based on piezoelectric impedance frequency shift, Appl. Sci. 6 (2016) 298, https://doi.org/10.3390/app6100298.
[22] M. Okugawa, K. Egawa, Study on smart washer using piezoelectric material for bolt loosening detection, J. JSNDI 52 (2003) 511–516.
[23] H. Yin, T. Wang, D. Yang, S. Liu, J. Shao, Y. Li, A smart washer for bolt looseness monitoring based on piezoelectric active sensing method, Appl. Sci. 6 (2016) 320, https://doi.org/10.3390/app6110320.
[24] L. Huo, D. Chen, Q. Kong, H. Li, G. Song, Smart washer – a piezoceramic-based transducer to monitor looseness of bolted connection, Smart Mater. Struct. 26 (2017) 025033, https://doi.org/10.1088/1361-665X/26/2/025033.
[25] B. Wang, L. Huo, D. Chen, W. Li, G. Song, Impedance-based pre-stress monitoring of rock bolts using a piezoceramic-based smart washer – a feasibility study, Sensors 17 (2017) 250, https://doi.org/10.3390/s17020250.
[26] V. Caccese, R. Mewer, S.S. Vel, Detection of bolt load loss in hybrid composite/metal bolted connections, Eng. Struct. 26 (2004) 895–906, https://doi.org/10.1016/j.engstruct.2004.02.008.
[27] R.A. Esmaeel, F. Tahari, Application of a simple and cost-effective method for detection of bolt self-loosening in single lap joints, Nondestruct. Test. Eval. 28 (2013) 208–225, https://doi.org/10.1080/10589759.2012.740042.
[28] J. Rivière, G. Renaud, S. Haupert, M. Talmant, P. Laugier, P.A. Johnson, Nonlinear acoustic resonances to probe a threaded interface, J. Appl. Phys. 107 (2010) 124901, https://doi.org/10.1063/1.3443578.
[29] Y. Huang, L. Liu, T. Yeung, Y. Hung, Real-time monitoring of clamping force of a bolted joint by use of automatic digital image correlation, Opt. Laser Technol. 41 (2009) 408–414, https://doi.org/10.1016/j.optlastec.2008.08.010.
[30] S.A. Nassar, A. Meng, Optical monitoring of bolt tightening using 3D electronic speckle pattern interferometry, J. Press Vess.-T. ASME 129 (2006) 89–95, https://doi.org/10.1115/1.2389024.
[31] F. Amerini, M. Meo, Structural health monitoring of bolted joints using linear and nonlinear acoustic/ultrasound methods, Struct. Health Monit. 10 (2011) 659–672, doi: 10.11771147592171039581O.
[32] F. Huda, I. Kajiwara, N. Hosoya, S. Kawamura, Bolt loosening analysis and diagnosis by non-contact laser excitation vibration tests, Mech. Syst. Signal Pr. 40 (2013) 589–604, https://doi.org/10.1016/j.ymssp.2013.05.023.
[33] J.J. Meyer, D.E. Adams, Theoretical and experimental evidence for using impact modulation to assess bolted joints, Nonlinear Dyn. 81 (2015) 103–117, https://doi.org/10.1007/s11071-015-1976-6.
[34] S.M. Parvasi, S.C.M. Ho, Q. Kong, R. Mousavi, G. Song, Real time bolt preload monitoring using piezoceramic transducer and time reversal technique –a numerical study with experimental verification, Smart Mater. Struct. 25 (2016) 085015, https://doi.org/10.1088/0964-1726/25/8/085015.
[35] T. Wang, L. Shaopeng, S. Junhua, L. Yourong, Health monitoring of bolted joints using the time reversal method and piezoelectric transducers, Smart Mater. Struct. 25 (2016) 025010, https://doi.org/10.1088/0964-1726/25/2/025010.
[36] Z. Zhang, M. Liu, Z. Su, Y. Xiao, Quantitative evaluation of residual torque of a loose bolt based on wave energy dissipation and vibro-acoustic modulation: A comparative study, J. Sound Vib. 383 (2016) 156–170, https://doi.org/10.1016/j.jsv.2016.07.001.
[37] Z. Zhang, M. Liu, Y. Liao, Z. Su, Y. Xiao, Contact acoustic nonlinearity (CAN)-based continuous monitoring of bolt loosening: Hybrid use of high-order harmonics and spectral sidebands, Mech. Syst. Signal Pr. 103 (2018) 280–294, https://doi.org/10.1016/j.ymssp.2017.10.009h.
[38] N. Hosoya, T. Hosokawa, I. Kajiwara, S. Hashimura, F. Huda, Evaluation of the clamping force of bolted joints using local mode characteristics of a bolt head, J. Nondestruct. Eval. 37 (2018) 75, https://doi.org/10.1007/s10921-018-0528-7.
[39] N. Hosoya, I. Kajiwara, K. Umenai, Dynamic characterizations of underwater structures using non-contact vibration test based on nanosecond laser ablation in water: investigation of cavitation bubbles by visualizing shockwaves using the Schlieren method, J. Vib. Control 22 (2016) 3649–3658, https://doi.org/10.1177/1077546314564693.
[40] N. Hosoya, R. Umino, I. Kajiwara, S. Maeda, T. Onuma, A. Mihara, Damage detection in transparent materials using non-contact laser excitation by nano-second laser ablation and high-speed polarization-imaging camera, Exp. Mech. 56 (2016) 339–343, https://doi.org/10.1007/s11340-015-0089-y.
[41] N. Hosoya, Y. Terashima, K. Umenai, S. Maeda, High spatial and temporal resolution measurement of mechanical properties in hydrogels by non-contact laser excitation, AIP Adv. 6 (2016) 095223, https://doi.org/10.1063/1.4964305.
[42] N. Hosoya, I. Kajiwara, K. Umenai, S. Maeda, Dynamic characterizations of underwater structures using noncontact vibration tests based on nanosecond laser ablation in water: evaluation of passive vibration suppression with damping materials, J. Vib. Control 24 (2018) 3714–3725, https://doi.org/10.1177/1077546317710158.
[43] N. Hosoya, R. Umino, A. Kanda, I. Kajiwara, A. Yoshinaga, Lamb wave generation using nanosecond laser ablation to detect damage, J. Vib. Control 24 (2018) 5842–5853, https://doi.org/10.1177/1077546316687904.
[44] N. Hosoya, S. Ozawa, I. Kajiwara, Frequency response function measurements of rotational degrees of freedom using a non-contact moment excitation based on nanosecond laser ablation, J. Sound Vib. 456 (2019) 239–253, https://doi.org/10.1016/j.jsv.2019.05.024.
[45] N. Hosoya, M. Nagata, I. Kajiwara, R. Umino, Nano-second laser-induced plasma shock wave in air for non-contact vibration tests, Exp. Mech. 56 (2016) 1305–1311, https://doi.org/10.1007/s11340-016-0167-9.
[46] Y. Zhang, T. Hiruta, I. Kajiwara, N. Hosoya, Active vibration suppression of membrane structures and evaluation with a non-contact laser excitation vibration test, J. Vib. Control 23 (2017) 1681–1692, https://doi.org/10.1177/1077546315599302.
[47] N. Hosoya, M. Mishima, I. Kajiwara, S. Maeda, Non-destructive firmness assessment of apples using a non-contact laser excitation system based on a laser-induced plasma shock wave, Postharvest Biol. Technol. 128 (2017) 11–17, https://doi.org/10.1016/j.postharvbio.2017.01.014.
[48] N. Hosoya, A. Yoshinaga, A. Kanda, I. Kajiwara, Non-contact and non-destructive Lamb wave generation using laser-induced plasma shock wave, Int. J. Mech. Sci. 140 (2018) 486–492, https://doi.org/10.1016/j.ijmecsci.2018.03.023.
[49] N. Hosoya, J. Kato, I. Kajiwara, Spherical projectile impact using compressed air for frequency response function measurements in vibration tests, Mech. Syst. Signal Process. 134 (2019) 10629, https://doi.org/10.1016/j.ymssp.2019.106295.